Journal of Alloys and Compounds 686 (2016) 616–627

Contents lists available at ScienceDirect

Journal of Alloys and Compounds

journal homepage: http://www.elsevier.com/locate/jalcom

Magnetic, structural and optical behavior of cupric oxide layers for solar cells

Dhanasekaran Vikraman [a, *], Hui Joon Park [a, b], Seong-Il Kim [c], Mahalingam Thaiyan [d]

[a] Division of Energy Systems Research, Ajou University, Suwon 16499, Republic of Korea
[b] Department of Electrical and Computer Engineering, Ajou University, Suwon 16499, Republic of Korea
[c] Nanophotonics Research Center, Korea Institute of Science and Technology, Hwarangno 14-gil 5, Seongbu-gu, Seoul 02792, Republic of Korea
[d] Department of Physics, Alagappa University, Karaikudi 630003, Tamilnadu, India

ARTICLE INFO

Article history:
Received 23 March 2016
Received in revised form
7 May 2016
Accepted 6 June 2016
Available online 11 June 2016

Keywords:
Nanomagnetism
Chemical synthesis
Nanosheets
Surface properties

ABSTRACT

Room temperature ferromagnetic hysteresis is observed in CuO nano films synthesized through chemical strategy. The room temperature ferromagnetic behavior in CuO is quite a new observation without any doping, annealing or any other post preparation treatments. The observed magnetization value is 0.24 T which is obviously depicted that the nano-scale magnetic properties dependent on the shape and size of nano films. The morphological observations is depicted that the uneven ellipsoidal grains transformed to nano-sheet shaped grains. Atomic force microscopy (AFM) images are also strengthening the observation of shape variations due to bath temperature variation. The surface profile and grain contour images are verified the size and shape variations. Structural variations are precisely predicted by X-ray diffraction patterns and crystallinity of the films is discussed. The growth mechanism of nano sheet formation and physical phenomena are discussed. The luminescence properties variations are observed by photo-luminescence (PL) spectroscopy and it has exposed that the bath temperature effects on the CuO films. X-ray photoelectron spectroscopy (XPS) spectra is depicted that Cu $2p_{3/2}$, Cu $2p_{1/2}$ and O_{1s} related peaks at 929.50, 952.80 and 529.38 eV binding energy, respectively. In addition, the optical dielectric dispersion parameters such as effective mass (m_e), optical susceptibility (χ_e), carrier concentration (N), plasma frequency (ω_p), relaxation time (τ) and frequency (f) are also evaluated. Raman scattering spectra revealed the A_g and B_g modes shift at 296 and 628 cm^{-1}.

1. Introduction

The discovery of new fascinating physical phenomena in the modern study of oxide materials is a vital research conception. The high-temperature superconductivity, colossal magnetoresistance, dilute magnetic doping, or multiferroicity were discovered and investigated in transition-metal oxides, demonstrating a prototype class of strappingly correlated electronic systems. This advance was accompanied by massive progress regarding thin film fabrication. The conventional semiconductor technology is approaching fundamental physical limits due to account of decreasing device dimensions. Making use of the spin of the electron as a degree of freedom additional to its charge opened the field of magneto- or spin electronics which is considered a replacement technology [1]. Starting from metal-based devices in the late 1980s, the field of spintronics soon expanded to transition metal oxide [2] and recently even to organic materials [3]. The high quality oxide based thin films and heterostructures are published in the past two decades and it has showed important advances concerning sample eminence. II–VI semiconductor based magnetic semiconductors have been studied for over two decades [2,4,5]. II–VI semiconductor based magnetic semiconductors have been studied for over two decades [6]. Among those systems that exhibit a peculiar magnetic behavior when they are reduced to the nanoscale, nano films of metals occupy an outstanding position. The statement of ferromagnetic-like performance in the surface modified Au, Ag and Cu NPs have attracted much attention, because of their potential in nanotechnology applications in addition to the fundamental physics concepts. It should be stated that the mentioned of ferromagnetism in Cu counterparts an important new proposal to this nanoscale system.

The magnetism and magnetic materials are intimately given the

* Corresponding author.
E-mail address: v.j.dhanasekaran@gmail.com (D. Vikraman).

http://dx.doi.org/10.1016/j.jallcom.2016.06.032
0925-8388/

prominent role in our daily life. The physicochemical conditions of the deposition conditions determine the dimension of the materials. Cupric oxide (CuO) is an imperative material because of optical band gap energy (1.1–1.5 eV), which is suitable for various devices like lenses and chemical and oil bases [7–10]. CuO is a promising material for the large-scale solar cell application with the theoretical maximum conversion efficiency of ~20%, because of its suitable bandgap (ideal for sunlight absorption), high optical absorption, abundance, and non-toxicity [11–14]. The various techniques are available for the deposition of metal oxide such as successive ionic layer adsorption and reaction (SILAR) [7], sputtering [15], thermal oxidation [16], evaporation [17], molecular beam epitaxy [18], and electrodeposition [19,20], etc. Among them SILAR technique is a promising technique because of its low cost and simple coating process. This low cost and innovative route was first reported by Ristov [21] and our group were previously reported on morphological properties and microstructural studies of cupric oxide thin films [22,23]. In recent times, Punnoose et al. [24] have prepared monoclinic CuO nanocrystals by the sol-gel method. Qin et al. have observed weak ferromagnetism (FM) up to 330 K for small nanograins which is lower than (D <) 10 nm, whereas the magnetic ordering for the CuO grains with D > 10 nm was essentially similar to the antiferromagnetic ordering of bulk CuO [25]. The room-temperature FM in CuO powders and thin films was observed by Qin et al. and they have predicted that the detected FM to be related to oxygen vacancies. Zhang et al. [26] and Wang et al. [27] have reported based on both the experimental and theoretical works that the surface oxygen vacancies of nanostructures play an important role in inducing room-temperature FM. Therefore, we have point out that the surface morphology of a material given the major role to be able to modulate room-temperature FM as a result of different surface areas. The relationship between surface morphology and FM is appreciated to explore in the range nanograins. However, the FM has been still a matter for strong debate, even though various ferromagnetic oxide semiconductors are reported so far. In order to examine the ferromagnetism carefully, several considerations on the evaluation from the experimental side are given. In the present study, we have reported that the FM inclusion in cupric oxide thin films due to the size decrement in grains and elaborate studies on optical properties variations.

1.1. Film growth and characterizations

Thin films of cupric oxide were grown by double dip SILAR technique using precursor solution bath encompassing 0.03 M copper sulphate and 0.06 M sodium hydroxide (Sigma Aldrich – 99% pure). The precursor bath temperature was varied from 75 °C to 95 °C and effects of bath temperatures were elaborately discussed for CuO thin films. The chemically etched glass substrates were cleaned using alcohol and acetone before using the deposition process. The pre-cleaned glass substrates were immersed in the precursor chemical bath for a known standardized time followed by immersion in hot solution maintained at 75–95 °C for the same time for hydrogenation. The phase one process of solution dip followed by phase two hot solution dipping is repeated for known number of times. The immersion time and number of immersion also varied to elucidate the properties variation of CuO films. Part of the CuO so formed was deposited onto the substrate as a strongly adherent film and the remainder formed as a precipitate. The schematic diagram of SILAR prepared CuO is given in Fig. 1. An X-ray diffractometer system [X'PERT PRO PANalytical, Netherlands] with Cuk_{α} radiation ($\lambda = 0.1540$) nm was used to identify the crystal structure of the films. Surface morphological study was carried out using a scanning electron microscopy (Philips Model XL 30, USA). The surface topology of the films was investigated by atomic force

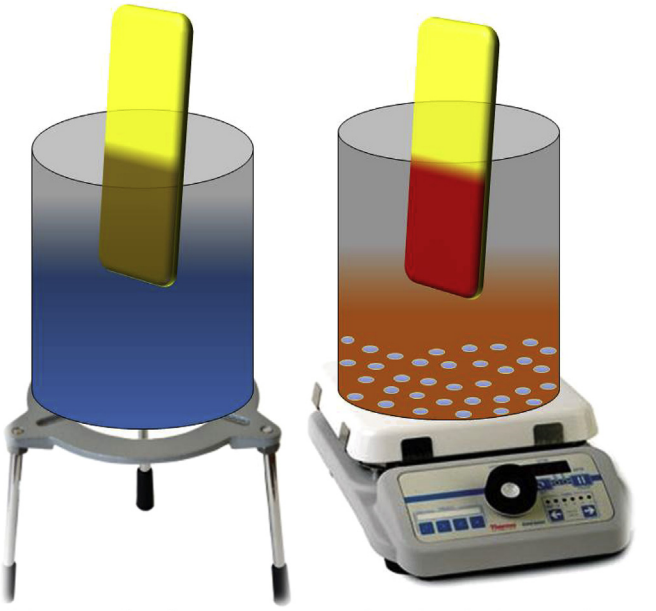

Fig. 1. Schematic representation of CuO formation by dipping method.

microscopy (Nanoscope E – 3138 J). Optical properties of the samples were analyzed using a UV–Vis–NIR double beam spectrophotometer (HR - 2000, M/S ocean optics, USA). Raman analyses were performed using Princeton Acton SP 2500 instrument through 0.5 focal length grating monochromator with 514.5 nm excitation line from Ar^{+} laser. X-ray photoelectron spectroscopy (XPS) studies were made by PHI 5000 Versa Probe. The Lakeshore, VSM 7410, vibrating sample magnetometer was used to analyze magnetic properties of nano films.

2. Results and discussion

2.1. Thickness studies

Fig. 2(a) defines rate of film thickness for SILAR grown CuO film as a function of immersion cycles such as 25, 50, 75 and 100, respectively. Film thickness is assessed against number of immersion cycles at bath temperatures ranging from 75 to 95 °C. The thickness rate linearly increases with increase of immersion cycle and get slowed down after 75 immersions. The rapid growth rate is observed up to 25 immersion cycles and it is exhibited at ~310 nm. The rich and translucent in the beginning of the deposition precursors is noted and it has crooked reddish-brown as escalation of immersion cycle. This is due to the formation of deferred oxides of Cu in the solution to form brown-black CuO. The solutions are substituted with fresh ones in the every 25 immersion cycle. The film growth rate is linearly increased from 25 to 75 immersion cycles and then slowly increased. The maximum value of film thickness is obtained at 540 nm for CuO nano films prepared at bath temperature 95 °C with 100 immersion cycles. Furthermore, variation of film thickness against number of immersion cycles for different deposition time ranging from 5 to 25 s of CuO thin films at bath temperature 95 °C in the supporting information Fig. S1. Progressively the film turns orange, red, brown, etc., due to optical interference under daylight. It is observed from the Fig. S1, film growth rate linearly increases with increase of immersion cycle and

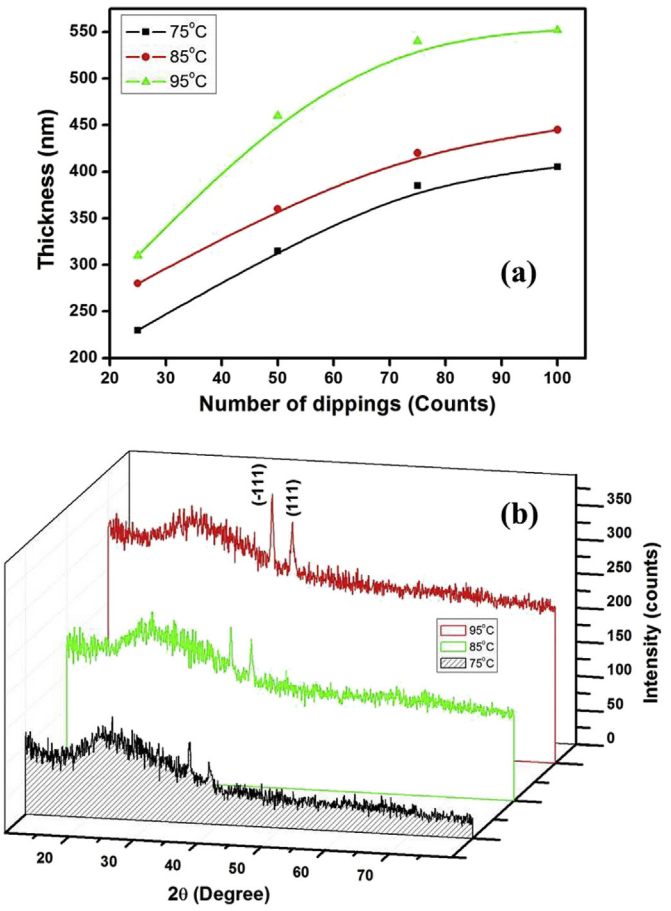

Fig. 2. (a) Film thickness variations as a function of number of immersions cycles of CuO thin films prepared at various bath temperatures; (b) X-ray diffraction patterns of various bath temperatures prepared CuO thin films.

gets slow down after 75 immersions. In the initial stage, the source materials are sufficient and the solution has high complexity. The process of deposition plays a more important role than the dissolution process which leads to increase in film thickness. With the deposition time being prolonged, the thickness of the film increases, at the same time the resistance of the film increases. Therefore, after a particular time of deposition, the dissolution process predominates over the deposition thereby resulting that decreases in film thickness. We noted that the solutions that were clear transparent in the beginning of the deposition, turned reddish-brown as the immersion cycles increased. This is due to the formation of suspended oxides of copper in the solution: yellow–orange CuO and brown black CuO. After about 25 immersion cycles, the solutions were substituted with fresh ones. The thickness of the films is rapidly increased from 25 immersions to 75 immersion cycles and then growth rate decreased moderately. The maximum value of film thickness is obtained at 540 nm at 95 °C prepared film with 100 immersion cycles. The rinsing step employed between the immersions in the SILAR process is meant to eliminate the transport of surface tension held solution layer to and fro the solution bath and hence avoids precipitation of semiconductor clusters and pigments in the bath. The reaction in such a case takes place only with the adsorbed ion layer leading to the deposition of thin films of relatively higher quality. From the above results, it has observed that rinsing time longer than 15 s couldn't yield higher film thickness. Hence, 15s in each of the solutions is chosen as the standard immersion period in the present case.

2.2. Structural studies

X-ray diffraction (XRD) patterns of various bath temperatures grown cupric oxide thin films are shown in Fig. 2(b). The observed diffraction patterns inter-planar spacing values are indexed with JCPDS values (# 89-5899). X-ray diffraction patterns revealed the polycrystalline nature of SILAR coated CuO films belonging to the monoclinic phase with (−111) preferential lattice orientation. The broad peak exhibited around the 2θ 25° due to the glass substrate for all the diffraction pattern of CuO. From the Fig. 2(b), the peak intensities are increased with increase of bath temperature which indicates an improvement of crystallinity of the prepared films. This improvement may be caused by the effective mass transfer and increased rate of deposition at higher temperatures. A (−111) peak position is located at $2\theta = 35.54^{\circ}$ corresponding to d-spacing value 0.2524 nm for CuO grown at bath temperature 95 °C. A blue shift is occurred in the diffraction angle of preferentially oriented plane in CuO as a function of bath temperatures. Also no other peaks are observed related to impurities. Fig. S2 (a–e) shows typical X-ray diffractogram of CuO films deposited at various rinsing time such as 5 s, 10 s, 15 s, 20 s and 25 s grown on glass substrates. The low intensity peak is observed at 5 s prepared cupric oxide thin films as shown in Fig. S2(a). The intensity of the peak increases with increase of rinsing time up to 15 s which is due to increase of film thickness. The diffraction peak intensity is also decreased for both of the reflection at above 15 s of rinsing time prepared films as shown in Fig. S2(c–e). The lattice parameters calculated for monoclinic crystal structure of films prepared at 15 s is 'a' = 4.684 Å, 'b' = 3.419 Å and 'c' = 5.134 Å. The high intensity of diffraction pattern is confirmed the improvement of crystallinity for CuO prepared at 15 s rinsing time as shown in Fig. S2(c). The blue shift is observed from 5 to 15sec of rinsing time and then red shifted. Fig. S3 shows that XRD patterns of CuO thin films prepared at different number of immersions ranging from 25 to 100. All the peaks are identified from CuO and hence no additional lines corresponding to Cu and O elements. The lower number of 25 immersion prepared film is amorphous state because there is no intense peak observed in the XRD pattern as shown in Fig. S3(a). The (−111) direction is the close packed direction of the cupric oxide structure and the deposited films are polycrystalline having the monoclinic CuO. These observations revealed that SILAR method is suitable for obtaining single phase CuO thin films. The observed lattice spacing (d = 2.5224 Å) value coincided with the standard JCPDS for monoclinic CuO.

X-ray diffraction analysis is carried out in order to determine the crystalline nature and microstructural properties of the films. Debye-Scherer's formula using full-width at half-maximum intensity (FWHM) expressed in radians

$$D = \frac{0.9\lambda}{\beta \cos\theta} \tag{1}$$

where D is crystallite size and β is the FWHM. The crystallite size can be controlled simply by varying the solution pH values. The microstrain ε was calculated from the slope of βcosθ vs sinθ plot using Equation (2),

$$\frac{\beta \cos\theta}{\lambda} = \frac{1}{D} + \frac{\varepsilon \sin\theta}{\lambda} \tag{2}$$

where λ is wavelength, D is crystallite size, β is FWHM of the predominant orientation and θ is Bragg's angle. The dislocation density δ defined as the length of dislocation lines per unit volume of the crystal and can be evaluated from the crystallite size 'D' by the relation:

$$\delta = \frac{n}{D^2} \tag{3}$$

where n is a factor, when equal unity giving minimum dislocation density. The relation connecting stacking fault probability (α) with peak shift Δ(2θ) was given by

$$\alpha = \left(2\pi^2/45\sqrt{3}\right)\left[\Delta(2\theta)/\tan\theta\right] \tag{4}$$

where D is crystallite size, β is full width at half maximum, α stacking fault probability and λ wavelength of the X-ray diffraction respectively. The texture coefficient (TC) values are calculated using relations,

$$T_C(h_ik_il_i) = \frac{I(h_ik_il_i)}{I_0(h_ik_il_i)}\left[\frac{1}{n}\Sigma\frac{I(h_ik_il_i)}{I_0(h_ik_il_i)}\right]^{-1} \tag{5}$$

where I_0 represents the standard intensity, I is the observed intensity of $(h_ik_il_i)$ plane and n is the reflection number.

The quantitative variation of microstructural parameters [28] for various bath temperatures grown CuO thin films is shown in Table 1. The crystallite size 'D' of the films is calculated from the Debye Scherer's formula Equation (1). The crystallite sizes are estimated as 17.9, 19.5 and 21.5 nm for films deposited at 75 °C, 85 °C and 95 °C, respectively. Table 1 indicates the increment of crystallite size with bath temperature and having maximum value of crystallite size for CuO film prepared at 95 °C bath temperature. This improvement may be due to the effective mass transfer and increased rate of deposition at higher temperatures. The bath temperature mainly affects the crystallite size of the film as reported by Li et al. [29]. Due to the release of defects in the lattice, the strain in the film gets released and attained its minimum value for film obtained at this bath temperature (95 °C). The dislocation density and microstrain values are calculated using Equations (2) and (3), respectively. The minimum value of microstrain is obtained at 2.35×10^{-3} lines^{-2} m^{-4} deposited at 95 °C bath temperature. An aggregate of distorted crystallites as a measure of the crystallite size and strain could affect the variance of the X-ray diffraction line profiles. The minimum value of dislocation density value 2.17×10^{15} lines/m^2 of CuO thin film prepared at 95 °C bath temperature. The stacking fault probability of SILAR prepared CuO thin films using expression given in Equation (4). The stacking fault is decreased as increase of bath temperatures due to the reduction of diffraction angles variations compared with standard values. The estimated values of stacking fault probability are tabulated in Table 1. Texture coefficient values are extracted using the relation 5. Table 1 represented that the maximum value of texture coefficient is observed for CuO thin film prepared at 95 °C and also the texture coefficient increased as increase of bath temperature. The texture coefficient value of predominant peak (−111) is found to be 1.22 at bath temperature 95 °C. It has been reported earlier that texture coefficient higher that 1 indicates preferential orientation and also indicates that abundance of grains in a given (h_i,k_i,l_i) direction. The type of conductivity of CuO thin films is due to the presence of Cu ion vacancies within the lattice. The studies on functional dependency of crystallite size, strain and dislocation density with bath temperature indicated that the strain and dislocation density decreases whereas the crystallite size increases. Similar behavior is reported to be exhibited by semiconducting thin films [30]. The elemental confirmation and oxidation states of the CuO thin films are analyzed using XPS. The O1s core level spectra is shown in Fig. 3(a), for different bath temperature prepared CuO. The observed peak at ~529.4 eV is due to the oxygen in the CuO lattices, which corresponds to the O–Cu bond [31]. The Cu 2p core-level spectrum (Fig. 3(b)) represents two peaks located at 933.5 and

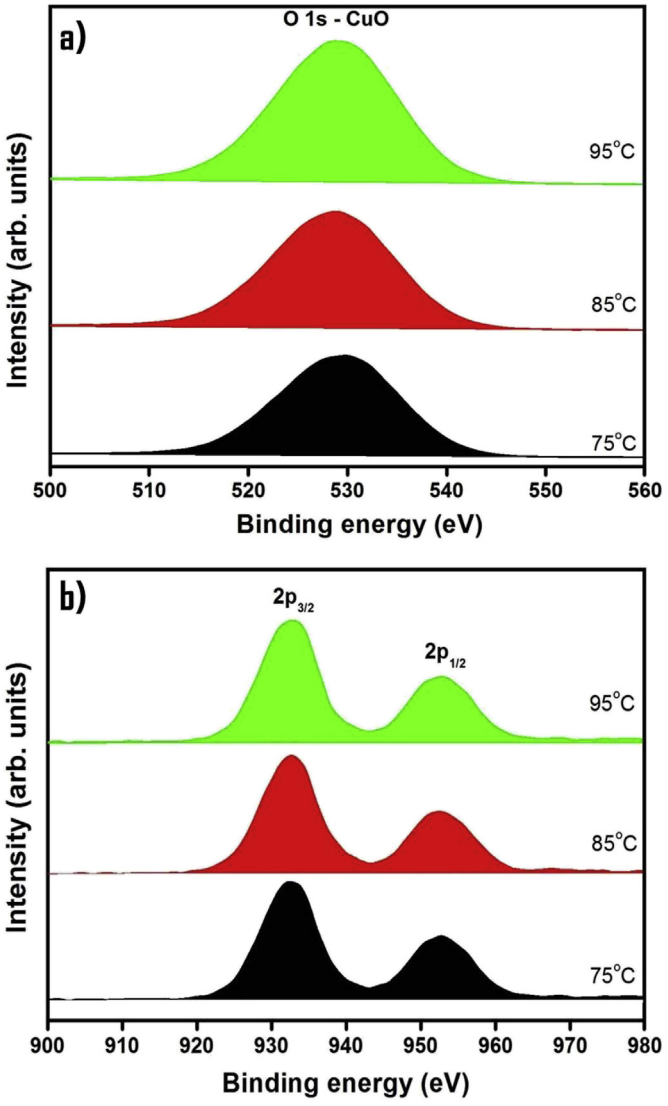

Fig. 3. XPS spectra of different bath temperatures prepared CuO films. (a) Cu and (b) O atoms-related binding energy.

Table 1
Microstructural parameters of SILAR prepared CuO thin films.

Bath temperatures (°C)	Crystallite size (nm)	Dislocation density (10^{15})	Microstrain (10^{-3})	Stacking fault probability (10^{-4})	Texture coefficient	
					−111	111
75	17.9	3.135	2.83	4.45	1.11	0.89
85	19.5	2.636	2.59	2.34	1.28	0.71
95	21.5	2.172	2.35	0.88	1.22	0.78

953.8 eV which corresponds to the Cu 2p3/2 and Cu 2p1/2, respectively. These values are consisted with the earlier reported values of Cu(2p) in CuO [31–34].

2.3. Morphological and topographical studies

The surface morphology of CuO thin films are examined by scanning electron microscopy (SEM). The typical micrograph of CuO thin film deposited at 75 °C (Fig. 4(a)) is revealed irregular surface comprising ellipsoidal granular regions. The undefined boundaries are observed in this micrograph with the hillocks and voids. Such type of morphology is undesirable for device applications. SEM image of a CuO thin film deposited at a bath temperature of 85 °C is shown in Fig. 4(b). The irregular shaped grains have been turned in to regular shape with elongated ellipsoidal like morphology. The well-defined boundary areas and surface homogeneity are observed as shown in Fig. 4(b). Also this morphological grain sizes are reduced with uniform surface. The nano sheet like morphology with regularly arranged surface is observed at 95 °C bath temperature prepared CuO as shown in Fig. 4(c). The grains are periodically arranged in sheet like structure in the nanoregime. These results indicated that are more compact with uniform grain structure due to the increase in nucleation over-growth. A decrease of crystallite size with bath temperature is also evident from SEM picture. The grain size is found to be substantially decreased for films deposited at higher bath temperature which may be due to the atoms are periodically arranged in the surface without any coalescence. Also the shapes of the grains are varied from elongated ellipsoidal grains to nano-sheet structure. This sheet like formation is exhibited due to the internal stress on the bath solution to react the film surface during dipping in the solution. In this stress can be dominate on the atoms arrangement while film formation. Hence, we have observed nano sheet like morphology observed by simple strategy bath temperature variation. This evolution can give more valuable insight into the surface formation process during the film growth. In this morphological variation could be emitted some marvellous properties on the surface of the film. As from our earlier discussion, room temperature FM has induced to the nano-sheet on the surface. This resulted in an increase in nucleation over-growth and the deposits are more compact with uniform grain structure.

Additionally, SEM images of CuO thin film prepared at 5 s rinsing time is shown in Fig. S4(a). Small nanosized grains are inconsistently distributed over smooth background for 5 s rinsing time prepared CuO. This clearly indicates that the nanocrystalline nature with smooth background may possess the slight amorphous phase of CuO thin film. The boundary of the film is not clearly predicted from the SEM micrograph. SEM image of 25 s rinsing time prepared film (Fig. S4b) evidently shows the morphological properties of CuO thin film. The grains are very small with unequal size and shape; also their boundaries are well defined. Also, some discontinuities and voids are observed in SEM image of Fig. S4(b). SEM micrograph of CuO thin films prepared at 50 and 75 immersions are shown in Fig. S5. The inhomogeneous morphology with coarse like structure is observed at 50 immersions as shown in Fig. S5(a). The more voids and lacking of grains are observed. The sheet shaped grains with inhomogeneous distribution is observed at 75 immersions as shown in Fig. S5(b). The voids and hillocks are observed due to the coalescence of grains.

Furthermore, we have investigated topological properties of cupric oxide thin films for the confirmation size decrement and shape variations. AFM topographical properties are extracted using WSxM software [35]. Fig. 5(a–c) shows that the topographs and

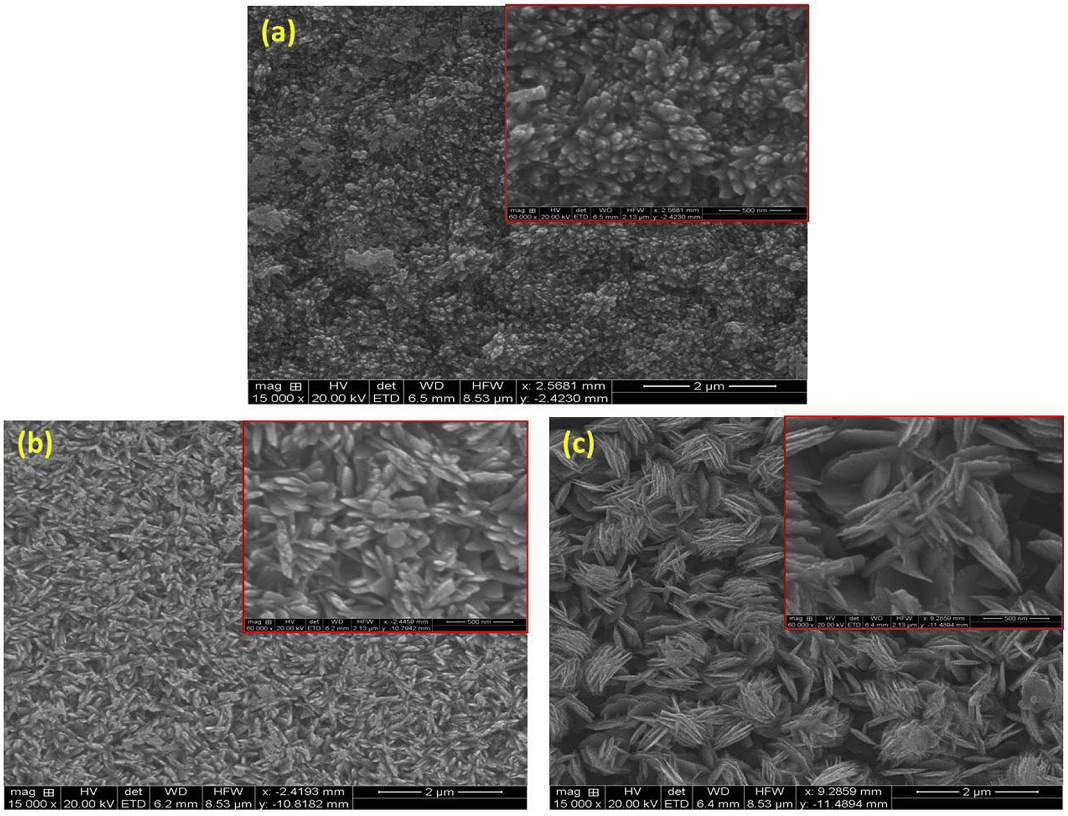

Fig. 4. Scanning electron micrographs of CuO thin films prepared at bath temperature (a) 75 °C, (b) 85 °C and (c) 95 °C; Inset figure shows higher magnification observed SEM micrographs for corresponding conditions.

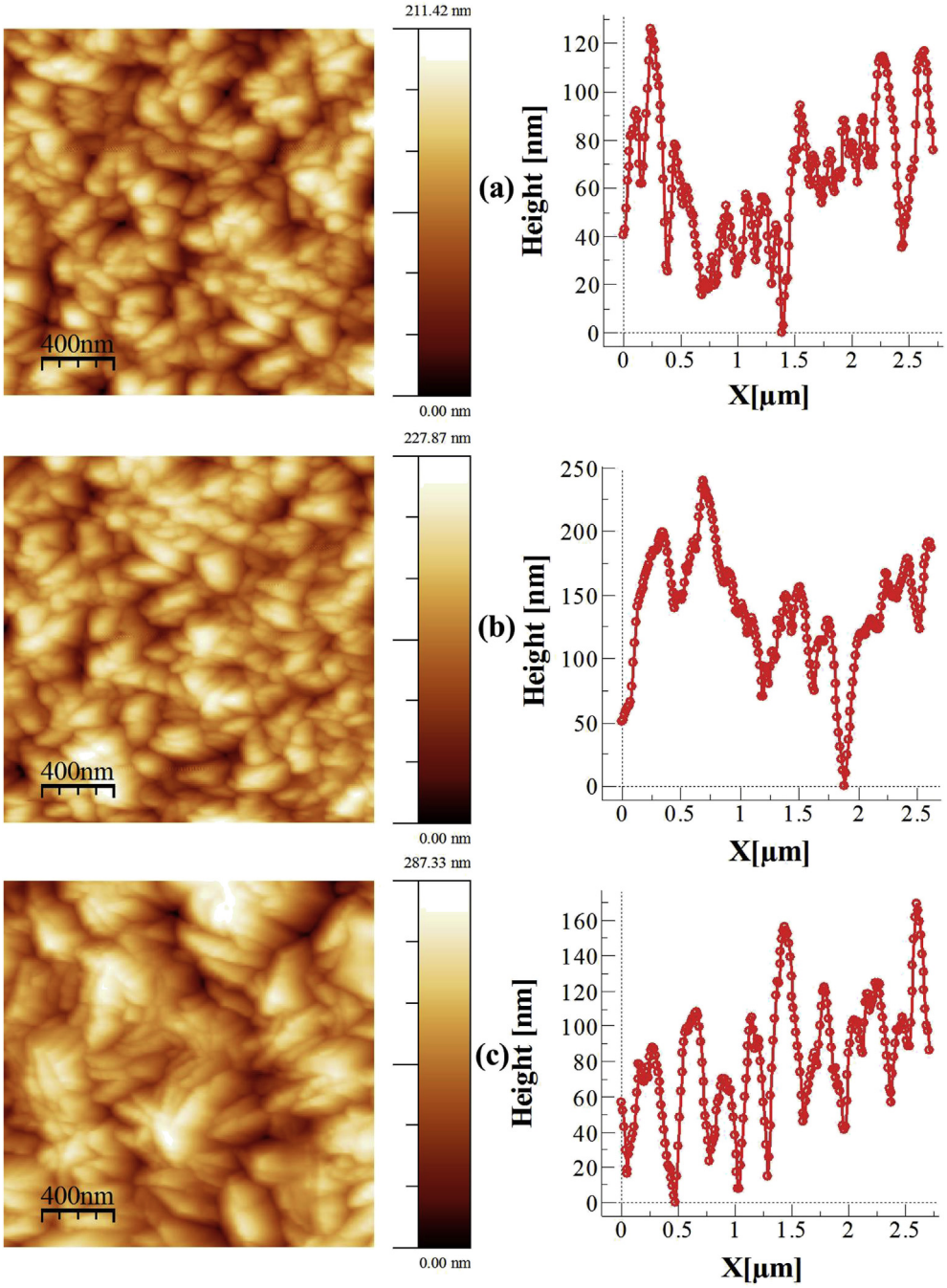

Fig. 5. AFM image and average grain size profile for CuO thin films prepared at different bath temperatures (a) 75 °C, (b) 85 °C and (c) 95 °C.

surface average grain size profile for different temperatures prepared CuO. Fig. 5(a) is clearly envisaged that the elongated ellipsoidal shaped grains observation in the surface for lower bath temperature prepared CuO film. Topographical image is exhibited with hillocks and voids between coalescence of grain bunch. The average grain size profile is represented that various sizes of grains formed on the film surface. Topographical image and grain size profile are presented in Fig. 5(b) for CuO thin film prepared at 85 °C bath temperature. Also, higher bath temperature prepared CuO topographical images are provided in Fig. 5(c). The nano-sheet shaped grains are observed in topographical 2D image of CuO thin film. CuO film is grown with densely packed and regular shaped grains as seen in the topograph. The sheet like layered structured is tuned by varying bath temperature for cupric oxide thin film. The grain size profile is indicated that average sizes of grains are exhibited in whole area of the film. The lower magnification topography and contours structure are provided in supporting Fig. S6. The lower number of dippings (75 immersions) and maximum time (25 s) prepared CuO thin films topographical images are provided in Fig. S7&S8 with the grain size profile spectra. The shape variations are obviously demonstrated from lower and higher bath temperature prepared CuO as shown in Fig. 4(a–c) and highly consisted SEM observations. The selectively oriented grains are exhibited some novel properties in the nano region. The shape and size variation could be reflected by possible reaction process in the SILAR grown CuO. CuO compound is designed by the combined

reaction of Cu^{2+} and $(OH)^{2-}$ during the dipping process. During the reaction process, excess of oxygen ions might be formed from the nucleation stage and it has occupied on the surface during the dipping process between the CuO atoms. Also, oxide ions might be affecting the uniform sheet shaped grains at the lower bath temperature. In this observation is exhibited due to the excess of oxygen ions involving the reaction with Cu ions at the lower bath temperature. The excess oxygen ions are stimulated to form coalescence of grains to interlink with one layer to another layer of grains in the lower bath temperature prepared film. Due to this excess of oxygen ions in the lower bath temperature surface structure is exhibited with undefined grains sizes and negotiable rate of strain is acting the surface during growth formation. When the bath temperature is increased, the surface layer of the film is designed by the uniform growth and it might be due to the number excess oxygen ions percentage is being deteriorated. So that we have observed mixer of sheet and elongated ellipsoidal shaped grains are observed in the 85 °C bath temperature prepared CuO surface. In this surplus oxygen content observation is exhibited in EDX analysis at lower bath temperature prepared CuO. When the bath temperature is increased in the maximum value at 95 °C, the surface of the film completely occupied by the sheet like structure and it is obvious evidence in SEM micrographs.

2.4. Optical studies

An optical transmission spectrum is used to study the optical properties of CuO nano films as shown in Fig. 6(a). The bath temperature is given eminent role to produce higher transmission exhibited in CuO nano films preparation. However, the maximum value of the transmittance is observed at NIR spectral region exceeds 70%. The film has a transmittance up to 48% for CuO prepared at bath temperature of 75 °C and it has increased up to 78% (840 nm) for 95 °C bath temperature coated CuO. The transmittance increases may be due to increase of film uniformity and crystallinity. It is evident that all the films have sharp absorption edges in the visible region and these absorption edges slightly shifted to shorter wavelengths (blue shift) when bath temperature is increased. In the UV region, the obvious absorption could be observed. The percentage of transmission is increased with the increase of film thickness as well as crystallite size decreased. This may be due to the metallic copper as interstitial atoms in the lattice of CuO crystallites, resulting in distortion of crystallites [36]. This feature can be enabled due to the copper and oxygen transfer and in some cases due to electron transfer to the conduction band. Beyond the absorption edge, broad peaks or adsorption bands occur at longer wavelength. Strong absorption bands in this region may be the results of intervalence transitions, and the weaker features are due to the intra-electronic d–d optical transitions. This may be due to the decrease in optical scattering because of grain growth, causing a reduction in the density of grain boundaries, which plays an important role in the scattering of these photons [37]. The regular arrangement of lower size crystallites could be easily transmit the incident light energy in the visible region.

The ability of a material to absorb light is measured by its absorption coefficient. The value of absorption coefficient for strong

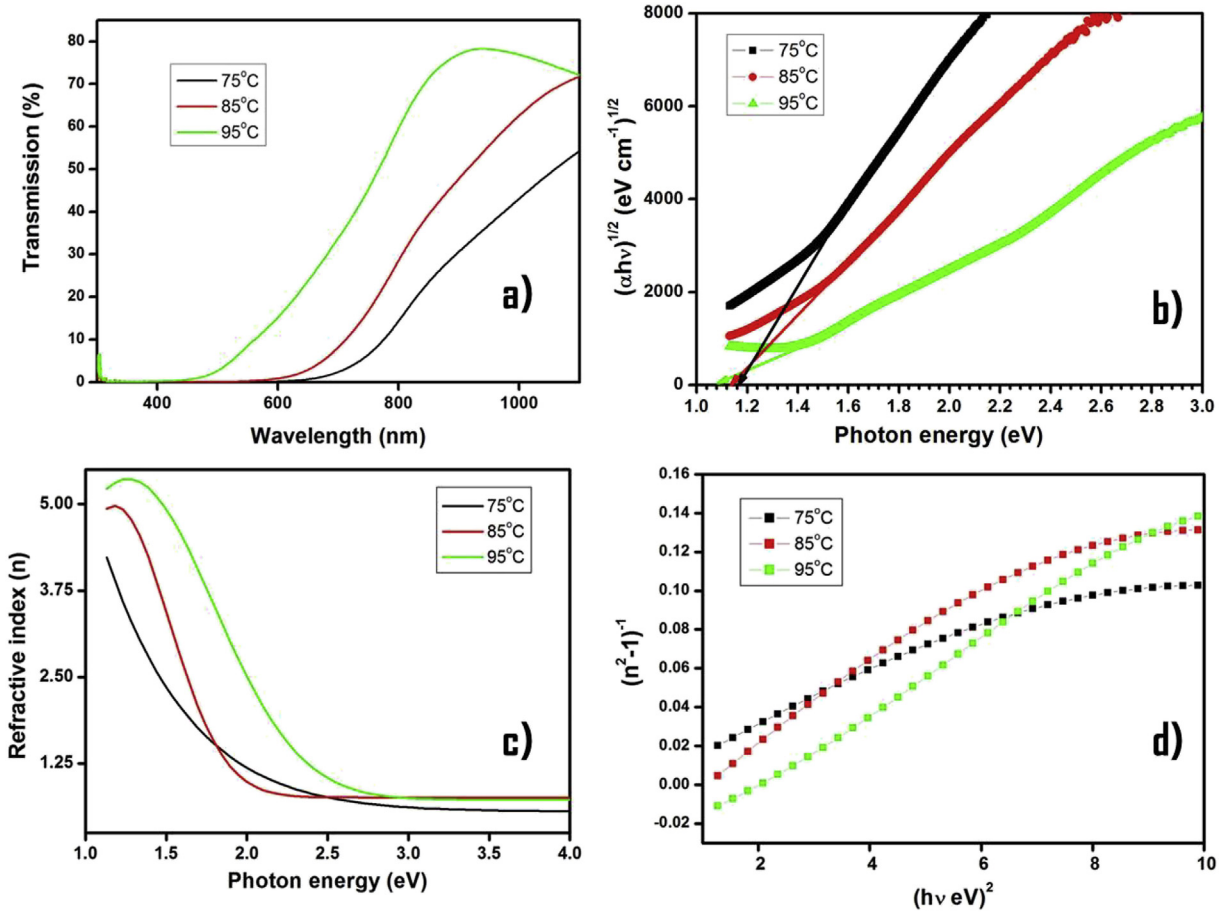

Fig. 6. (a) Optical transmission versus wavelength (b) Tauc's plot (c) Refractive index versus photon energy and (d) Plot of $(h\nu)^2$ vs $(n^2-1)^{-1}$ of different bath temperatures prepared CuO thin films.

absorption region of thin film is calculated using the previous report [38]. Extrapolation of plot to the *x*-axis gives the band gap energy of CuO film (Fig. 6(b)). The indirect band gap energy of CuO thin film is found to be 1.08 eV at optimized bath temperature and this value is in good agreement with earlier report. Optical band gap values are slightly varied with bath temperature it may due to crystallite size and uniformity of the films. The XRD result shows that increment of crystallite size with bath temperature is correlated with reduction of optical band gap. Also this reduction of band gap is mainly due to the sp–d exchange interactions between the band electrons of CuO and the localized d electrons of the Cu-ions which arise as these ions replace Cu^{2+} ions. A shift in band gap from higher energies to lower energies is observed as well as film thickness is increased with bath temperature. The crystallite size and strain are given predominant role to shift band gap energy from higher to lower. It is evident that indirect band gap shift towards lower energy with increase in crystallite sizes. The band gap is decreased from 1.16 to 1.08 eV in 27–21 nm of crystallite size for 75–95 °C bath temperature prepared CuO nano films, respectively. It is attributed to the presence of inter gap defect states in CuO nano films that act to lower the optical band gap [39]. It is well known that the optical properties of the copper monoxide are strongly affected by the type and concentration of defects in the sample [40]. The structure of CuO is known to have several defects such as oxygen and Cu vacancies [40,41]. However, this effect becomes more pronounced in the electric and optical performances of the film as film thickness increases.

Fig. 6(c) is exposed to refractive index (n) variation as a function of photon energy for various bath temperatures prepared CuO thin films. Transmission spectrum is used to calculate the refractive index using a modified algorithm of the envelope method proposed by Swanepoel [42]. The refractive index is decreased with bath temperatures which are attributed due to increase of crystallite size and decrease of microstrain with more appreciable bath temperatures variation in the steps of 10 °C. The cupric oxide films extinction coefficient (k) value is estimated using an expression [20]. Fig. S9(a) shows that variation of extinction coefficient of CuO thin films as a function of photon energy. The extinction coefficient is decreased for CuO thin films as a function of photon energy which may due to the increase of absorption coefficient [43]. The refractive indices reductions might be due to the close packing nature of the grains as coalesce of grains caused the densification of the layers with increase of bath temperatures. These results are suggested that the CuO films exhibited at normal dispersions in the UV–Vis–NIR region. The earlier report has more close agreement with our proposed results [44,45].

The variations of complex dielectric constant values of CuO thin films prepared at various bath temperatures is presented in supporting Fig. S9(b,c). The calculated imaginary and real parts of the dielectric constant are directly related to the density of states within the forbidden gap of the investigated oxides [46–48]. The dielectric constants are linearly decreased as a function of photon energy of various bath temperatures prepared CuO thin films. It has seen that both ε_1 and ε_2 decreases with increase of photon energy. The complex dielectric constant values are decreased with increase of bath temperature, which may be due to the reduction of grain boundaries thereby changing the structure and morphology of the surface. It has been well established that the complex dielectric constant clampdown as the size of quantum confined physical systems in the nanometric range [46]. Also, the observation of dielectric suppression directly related with atomic coordination-number imperfection, which dictates that the size dependence of the atoms orientation and electron-phonon coupling, thus determines the entire band structure such as band gap reduction or expansion.

The frequency dependent dielectric constants are defined using "dispersion energy" parameters E_d and E_0 by Wemple and Di-Domenico model [49,50].

$$n^2 = 1 + \left(\frac{E_0 E_d}{E_0^2 - (h\nu)^2}\right) \tag{6}$$

where E_0 is the energy of the effective dispersion-oscillator n is the refractive index, "$h\upsilon$" is the incident photon energy and E_d is called dispersion energy, which measures the average strength of inter-band optical transitions. Wemple and Di-Domenico were proposed to fit the refractive index dispersion values with photon energy for the prepared films. The dispersion plays an important role in the research for optical materials, because it is a significant factor in optical communication and in designing devices for spectral dispersion. Although these rules are quite different in detail and iconicity influence the refractive index behavior of solids in ways that can be simply described [49]. Wemple and Di-Domenico have analyzed different solids and liquids using a single effective-oscillator fit of the form [50]. The model describes dielectric response for transitions below the optical gap values. The spectral dependence of refractive index in semiconductors can be evaluated using the single oscillator model proposed by Wemple and Di-Domenico and also these models have been widely studied in recent years [51–53]. Experimental verification of Equation (6) can be obtained by plotting $(n_2-1)^{-1}$ vs. $(h\upsilon)^2$ as illustrated in Fig. 6(d). E_0 and E_d values are determined from the slope, $(E_0E_d)^{-1}$ and intercept (E_0/E_d), on the vertical axis and given in Table 2. The point of interception with the extrapolate at $(h\upsilon)^2 = 0$ yield the value of the dielectric constant at higher wavelength. The obtained values of CuO thin film deposited at different bath temperatures is given in Table 2. The high frequency dielectric constant is connected with contribution of the electronic polarization mechanism to the total dielectric response of CuO thin films. The E_0 value is increased and E_d value is decreased for CuO thin films as increase of bath temperature. The E_0 and E_d values are 2.64 eV and 4.69 eV for CuO thin film prepared at 95 °C bath temperature.

$$f_s = E_0 E_d \tag{7}$$

The oscillator strength (f_s) is given by Wemple and Di-Domenico [49]. The obtained values of "f_s" for different bath temperatures prepared CuO is given in Table 2. On the other hand, the parameters of the single-oscillator model E_0 and E_d are connected to M_{-1} and M_{-3} moments of the optical spectra, through the two relations [51,53].

$$E_0^2 = \frac{M_{-1}}{M3}$$
$$E_d^2 = \frac{M_{-1}^3}{M3} \tag{8}$$

The expression 8 indicates a single-oscillator approximation to the dielectric response of these materials. The dispersion moments of M_{-1} and M_{-3} are calculated from the data on E_0 and E_d as given in Table 2. The obtained M_{-1} and M_{-3} moments are slightly changed with bath temperatures variation. The dispersion parameters of M_{-1} and M_{-3} values are 1.774 eV and 0.253 eV^2, respectively for CuO thin film prepared at higher bath temperature. The optical moments are related to the macroscopic quantities like effective dielectric constant, effective number of valence electrons in the investigated material [54].

Table 2
Dispersion parameters of SILAR prepared CuO thin films.

Bath temperature (°C)	Dispersion parameters				Oscillator strength $(eV)^2$	Energy band gap eV
	M_{-1}	M_{-3} $(eV)^2$	E_0 (eV)	E_d (eV)		
75	2.339	0.363	2.53	5.93	89.48	1.12
85	2.145	0.360	2.44	5.24	66.92	1.09
95	1.774	0.253	2.64	4.69	58.31	1.08

$$\varepsilon = \varepsilon_\infty - \left(\varepsilon_\infty \omega_p^2\right)/\omega^2 \tag{9}$$

$$\omega_p^2 = \left(4\pi N e^2\right)\left(m_e^* \varepsilon^\infty\right) \tag{10}$$

where, ε_∞ is static dielectric constant, ω_p is plasma frequency m_e^* is electron reduced mass and N is carrier concentration. The plasma frequency has been calculated from the complex dielectric constant whose expression is given above [55]. The estimated values of ε_∞ (Table 3) is varied between 5.17 and 2.68 while the values of ω_p is varied (Table 3) between 6.01 and 6.32 × 10^{15} s^{-1} for the films deposited with different bath temperatures. In a semiconductor, carrier concentration (N) varies according to the square of plasma frequency ω_p as given in Equation (10) [56]. We can estimate carrier concentration of CuO thin films using the relation 11 [56]. The carrier concentration value is about 4.83 × 10^{20} cm^{-3} of CuO thin film prepared at higher bath temperature. If the carrier concentration is known, the effective mass of the charge carriers could be found out from the plasma frequency. It is observed from the Table 3, effective mass and carrier concentrations tend to increase as decrease of band gap energies. The lower effective mass value is calculated about 0.901 for CuO thin film prepared at 95 °C. The contribution from the free carrier electric susceptibility (χe), to the real dielectric constant is discussed according to the Spitzer–Fan model by Ref. [57].

$$\varepsilon_r = n^2 - k^2 = \varepsilon_\infty - \left[e^2/\pi c^2\right](N/m^*)\lambda^2 \tag{11}$$

$$\left[e^2/\pi c^2\right](N/m^*)\lambda^2 = -4\pi\chi_e \tag{12}$$

where ε_∞ is the high-frequency dielectric constant in the absence of any contribution from free carriers, χ_e is the electric free carrier susceptibility, N/m^* is the carrier concentration to the effective mass ratio, e is the electronic charge, and c is the velocity of light. Table 3 is demonstrated that the optical susceptibility values of cupric oxide thin films for different bath temperatures. A good fit to a straight line is seen from the free carrier susceptibility values at the extremes of the investigated range. Table 3 depicted that "χ_e" increases in magnitude with the bath temperatures and becomes sufficiently large to reduce the refractive index and dielectric constant. The dielectric relaxation time "τ" can be evaluated by using the relation [58].

$$\varepsilon_2 = \left(\varepsilon_\infty \omega_p^2/8\pi^2 c^3 \tau\right)\lambda^3 \tau = {}^1/\gamma_p = \varepsilon_1 - \varepsilon_\infty/\omega\varepsilon_2 \tag{13}$$

From the Equation (13) we have to calculate relaxation time. Table 3 indicates the dielectric relaxation time "τ" as a function of bath temperatures. This is represented that the relaxation time increases with increasing the bath temperatures. The variation of frequency of the investigated films with frequency "f" is tabulated in Table 3. The frequency of CuO thin film is estimated about 1.02 × 10^{13} s prepared at higher bath temperature. It is found that the frequency increases with increasing bath temperatures for due to increase of optical absorption region.

2.5. Raman, electrical and magnetic properties

Raman spectroscopy is known to be a very useful tool for monitoring the structural order–disorder degree at short range and crystallinity of oxide materials. The C^6_{2h} space group monoclinic CuO drives with two molecules per unit cell. There are nine zone centers in optical phonon modes with symmetries of 4Au + 5Bu + Ag + 2Bg [59,60]. It is well known that a number of physical properties of materials depend on the interactions between vibrational modes of molecules or lattices. In order to obtain information on such interactions in CuO nano films, it is necessary to investigate the way in which the lattice vibration wavenumbers vary with bath temperature (Fig. 7). A broad peak with a relatively high intensity at 297 cm^{-1} is assigned to Ag band, and other peak at 628 cm^{-1} is assigned to B_g as shown in Fig. 7. Raman active modes related peaks of CuO nano films are in good agreement with earlier reports. It has been observed that the scattering of local transverse optical phonons leads to a broad Raman band at around 297 cm^{-1}. These significant peak intensities indicate the single phase property and high crystallinity of leaves-like CuO structures. The peak broadens and shifts to the lower frequency side as the size of the crystallites decreases [61]. When the grain size increases in higher bath temperature prepared CuO nano films, the Raman peaks were found at 295.5 and 627 cm^{-1}, in agreement with the results of bulk CuO.

The low temperature electrical resistance measurement is carried out in the temperature range 150–400 K using the DC two-point probe method. The resistivity of a CuO film was found to be 79 MΩ-cm at room temperature. Fig. S10 shows the variation of log of resistivity (ln ρ) with reciprocal of temperature (1/T) × 10^3. The conduction activation energy was calculated using the following relation,

Table 3
Dielectric properties of SILAR prepared CuO thin films.

Bath temperature (°C)	Static dielectric constant (ε_∞)	Plasma frequency (10^{15}) s^{-1}	Effective mass (m_e)	Carrier concentration (10^{20}) cm^{-3}	Frequency (10^{13}) Hz	Relaxation time (10^{-14}) s	Optical susceptibility χ_e
75	5.17	6.01	0.904	5.20	3.55	2.81	0.56
85	4.97	6.61	0.902	6.25	1.34	7.42	0.62
95	2.68	6.32	0.901	4.83	1.02	9.76	0.68

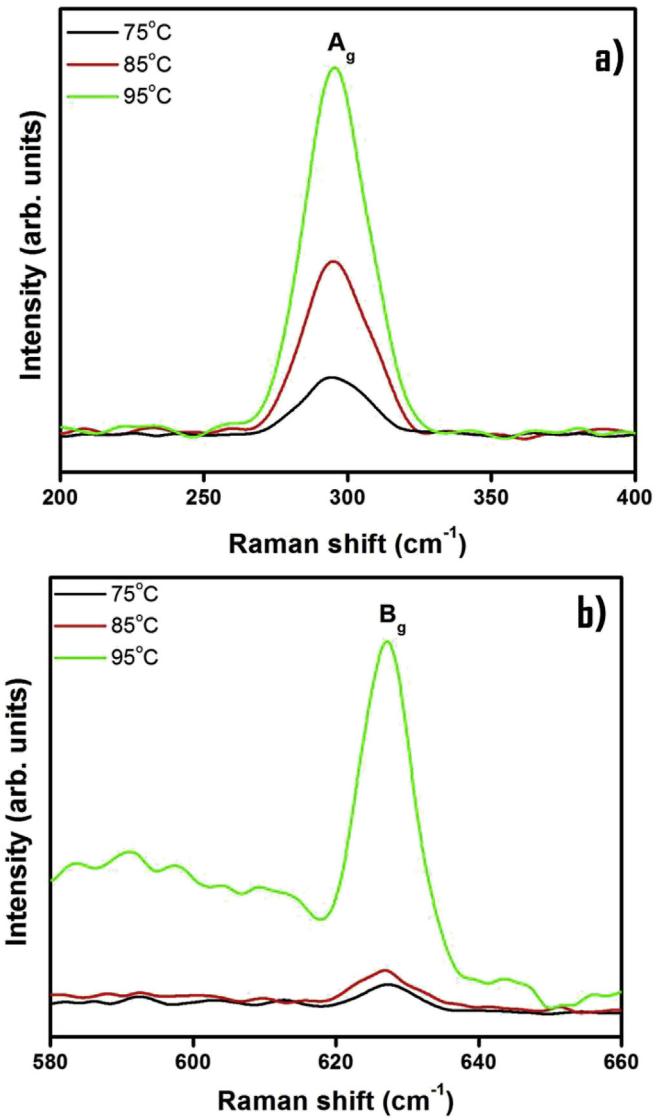

Fig. 7. Raman shift variations of CuO thin films prepared at different bath temperatures for (a) A_g mode and (b) B_g mode vibrations.

$$\sigma = \sigma_0 \exp\left(\frac{-E_g}{KT}\right) \quad (14)$$

where σ0 is a constant, E_g is the resistivity activation energy, K is the Boltzmann constant, T is an absolute temperature and is the conductivity, respectively. The activation energy obtained from the linear portion of the graph was found to be 0.29 eV. These tail bands are formed by localized electronic states; they are separated from extended states in the bands by a mobility edge. The electrical activation energy is related to the energy necessary to delocalize charge carriers through electronic transitions from localized states towards extended states. Recently, a highly crystalline CuO film possessing a resistivity of 3.3×10^5 Ω cm reported by Zhu et al. [10]. The activation of the intrinsic electrical conductivity in semiconductor like materials may be also explained by thermal excitation from valence band to conduction band.

The magnetic properties of cupric oxide nano films are analyzed using vibrating sample magnetometer. The magnetic hysteresis loop of CuO nano films synthesized at various bath temperatures is shown in Fig. 8. The ferromagnetic behavior is not induced in CuO thin films prepared at 75 °C bath temperature which possess larger grain sizes. The observed M − H behavior of CuO thin films prepared at 75 °C bath temperature reveals a mixture of ferromagnetic and diamagnetic phases. The hysteresis loop of CuO thin film is found to be narrow. However, M − H behavior of CuO thin films prepared at higher bath temperatures such as 85 °C and 95 °C reveals ferromagnetic behavior as observed in Fig. 8. The inset figure is clearly representing the magnetization values variations with bath temperature. The saturation magnetization values are estimated to be 0.22 and 0.24 T for 85 and 95 °C prepared CuO, respectively. Also the observed coercivity value is 355.5 O_e for higher bath temperature prepared CuO. The increase in magnetization with the decrease in grain size for CuO nano films has been attributed to an enhancement in the uncompensated surface spins [24]. The saturation magnetization increases significantly with increase of bath temperature. This clearly indicates that nano scale grains enhance ferromagnetic coupling. In the case of ferromagnetic nano structures, the moment corresponds to the core of the particle and surface spin acts as disordered collection of spins. Hence, it leads to the prediction that the reduction of particle size increases the surface to volume ratio which in turn increases the net magnetization. Similar behavior has been observed in several nonmagnetic metallic oxide nano particle systems [62]. Magnetic nanostructures exhibit properties that are different from their bulk counter parts due to the extremely small size of the nano particles. The donor impurity states induced by the native defects, such as the oxygen vacancies, are also essential to the magnetization of oxide-based magnetic semiconductors [63]. However, recently reported research work emphasizes that some traditional antiferromagnetic materials indeed exhibit ferromagnetic behavior when the size was decreased to nano scale, such as CuO, NiO, and MnO nanoparticles show typical hysteresis loop below bulk Neel transition temperature [64–66].

Ferromagnetic-like behavior at RT was also observed in other semiconductor such as CdSe:Cu and thiol-capped CdSe [67]. Sundaresan et al. [68] have reported earlier room temperature ferromagnetic behavior in In_2O_3, CeO_2, ZnO, Al_2O_3 and SnO_2. Therefore, we believe that another mechanism in addition to the film morphology might contribute to the enhancement of FM in the CuO. Based on the observation of theoretical analysis, RT ferromagnetism appeared for non-magnetic doped and undoped

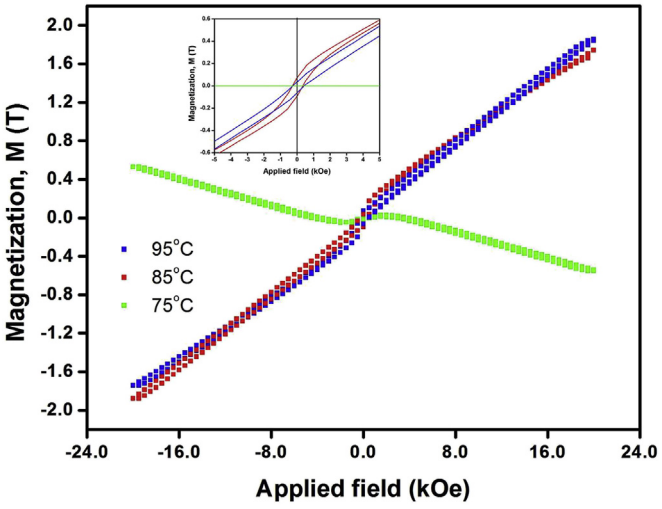

Fig. 8. M-H hysteresis spectra of CuO thin films synthesized at various bath temperatures; Inset figure shows the magnified portion of coercive force.

samples. These analyses were carried out by Sanchez et al. [69] for wurtzite ZnO. These studies are not only limited to ZnO and may be extended to other metal oxides based on the preparation route with selective structures. The important conclusion that we derive from our present work is that surface modification can deeply alter the magnetic properties of systems by changing the electronic structure of the nano films. As the crystallites are reduced to nanometer size the surface/volume ratio increases and hence the role of the surface in the magnetic behavior becomes increasingly important.

3. Conclusions

Monoclinic phase (−111) oriented cupric oxide thin films were successfully prepared by SILAR technique at various bath temperatures. The refractive index (n) and absorption index (k) are computed from the obtained T(λ) using Swanepoel's method. The optical band gap is calculated in terms of Tauc's method. Spectrophotometer data revealed that the optical transmittance increased slightly and the bang gap decreased from 1.16 to 1.08 eV with increasing bath temperature. Moreover, the intercrystallite stress could be relaxed by increasing the crystallite size and crystallinity of CuO thin films. The optical band gap decreases with increasing grain size and thickness. The type of optical transition responsible for optical absorption was indirect transitions. The relaxation time (τ) and plasma frequency (ε_p) of CuO thin film are found to increase with bath temperatures. The parameters like plasma frequency, carrier concentration and effect mass are estimated to be 6.32×10^{14} s^{-1}, 4.83×10^{20} cm^{-3} and 0.901, respectively, for films synthesized at optimized bath temperature. The electrical properties are discussed for 95 °C prepared CuO thin film. The near stoichiometric composition is observed at higher bath temperature prepared CuO thin film which is confirmed by using EDX analysis. The detailed investigation of morphological properties is done by SEM. Raman scattering is indicated the Ag and Bg mode vibration peak for CuO nanofilms. Room temperature FM behavior with a higher magnetization is observed which may be due to the nanoleaves in the surface of the films. In view of the interesting room temperature ferromagnetic behavior, CuO semiconductor is likely to play key role in future electronic devices.

Acknowledgement

This work was supported by the Basic Science Research Program through the National Research Foundation of Korea (NRF), funded by the Ministry of Education (NRF-2014R1A1A2056403), the Ministry of Trade, Industry & Energy (MOTIE, 10051565) and Korea Display Research Corporation (KDRC) support program for the development of future devices technology for the display industry..

Appendix A. Supplementary data

Supplementary data related to this article can be found at http://dx.doi.org/10.1016/j.jallcom.2016.06.032.

References

[1] G.A. Prinz, Magnetoelectronics, Science 282 (1998) 1660–1663.
[2] S.B. Ogale, Thin Films and Heterostructures for Oxide Electronics, Springer Science & Business Media, 2006.
[3] S. Sanvito, Molecular spintronics, Chem. Soc. Rev. 40 (2011) 3336–3355.
[4] M. Bibes, A. Barthelemy, Oxide spintronics, electron devices, IEEE Trans. 54 (2007) 1003–1023.
[5] M. Bibes, J.E. Villegas, A. Barthelemy, Ultrathin oxide films and interfaces for electronics and spintronics, Adv. Phys. 60 (2011) 5–84.
[6] W. Giriat, J. Furdyna, R. Willardson, A. Beer, Semiconductors and Semimetals, 25, Academic, Boston, 1988, p. 1.
[7] V. Dhanasekaran, T. Mahalingam, Surface modifications and optical variations of (− 111) lattice oriented CuO nanofilms for solar energy applications, Mater. Res. Bull. 48 (2013) 3585–3593.
[8] M. Norman, A. Freeman, Model supercell local-density calculations of the 3 d excitation spectra in NiO, Phys. Rev. B 33 (1986) 8896.
[9] J.-Z. Xu, J.-J. Zhu, H. Wang, H.-Y. Chen, Nano-sized copper oxide modified carbon paste electrodes as an amperometric sensor for amikacin, Anal. Lett. 36 (2003) 2723–2733.
[10] C. Zhu, M.J. Panzer, Seed layer-assisted chemical bath deposition of cuo films on ITO-Coated glass substrates with tunable crystallinity and morphology, Chem. Mater. 26 (2014) 2960–2966.
[11] S. Masudy-Panah, G.K. Dalapati, K. Radhakrishnan, A. Kumar, H.R. Tan, Reduction of Cu-rich interfacial layer and improvement of bulk CuO property through two-step sputtering for p-CuO/n-Si heterojunction solar cell, J. Appl. Phys. 116 (2014) 074501.
[12] S. Masudy-Panah, G.K. Dalapati, K. Radhakrishnan, A. Kumar, H.R. Tan, E. Naveen Kumar, C. Vijila, C.C. Tan, D. Chi, p-CuO/n-Si heterojunction solar cells with high open circuit voltage and photocurrent through interfacial engineering, Prog. Photovolt. Res. Appl. 23 (2015) 637–645.
[13] S. Masudy-Panah, K. Radhakrishnan, H.R. Tan, R. Yi, T.I. Wong, G.K. Dalapati, Titanium doped cupric oxide for photovoltaic application, Sol. Energy Mater. Sol. Cells 140 (2015) 266–274.
[14] F. Gao, X.-J. Liu, J.-S. Zhang, M.-Z. Song, N. Li, Photovoltaic properties of the p-CuO/n-Si heterojunction prepared through reactive magnetron sputtering, J. Appl. Phys. 111 (2012) 084507.
[15] C.L. Carnes, J. Stipp, K.J. Klabunde, J. Bonevich, Synthesis, characterization, and adsorption studies of nanocrystalline copper oxide and nickel oxide, Langmuir 18 (2002) 1352–1359.
[16] S. Ghosh, D. Avasthi, P. Shah, V. Ganesan, A. Gupta, D. Sarangi, R. Bhattacharya, W. Assmann, Deposition of thin films of different oxides of copper by RF reactive sputtering and their characterization, Vacuum 57 (2000) 377–385.
[17] Y. Gong, C. Lee, C. Yang, Atomic force microscopy and Raman spectroscopy studies on the oxidation of Cu thin films, J. Appl. Phys. 77 (1995) 5422–5425.
[18] L. Huang, S. Yang, T. Li, B. Gu, Y. Du, Y. Lu, S. Shi, Preparation of large-scale cupric oxide nanowires by thermal evaporation method, J. Cryst. Growth 260 (2004) 130–135.
[19] Z. Yu, C.M. Wang, M.H. Engelhard, P. Nachimuthu, D.E. McCready, I. Lyubinetsky, S. Thevuthasan, Epitaxial growth and microstructure of Cu2O nanoparticle/thin films on SrTiO3(100), Nanotechnology 18 (2007) 115601.
[20] V. Dhanasekaran, T. Mahalingam, R. Chandramohan, J.-K. Rhee, J. Chu, Electrochemical deposition and characterization of cupric oxide thin films, Thin Solid Films 520 (2012) 6608–6613.
[21] M. Ristov, G. Sinadinovski, I. Grozdanov, Chemical deposition of Cu 2 O thin films, Thin solid Films 123 (1985) 63–67.
[22] V. Dhanasekaran, T. Mahalingam, V. Ganesan, SEM and AFM studies of dip-coated CuO nanofilms, Microsc. Res. Tech. 76 (2013) 58–65.
[23] V. Dhanasekaran, T. Mahalingam, Physical properties evaluation of various substrates coated cupric oxide thin films by dip method, J. Alloys Compd. 539 (2012) 50–56.
[24] A. Punnoose, M. Seehra, Hysteresis anomalies and exchange bias in 6.6 nm CuO nanoparticles, J. Appl. Phys. 91 (2002) 7766–7768.
[25] H. Qin, Z. Zhang, X. Liu, Y. Zhang, J. Hu, Room-temperature ferromagnetism in CuO sol–gel powders and films, J. Magnetism Magnetic Mater. 322 (2010) 1994–1998.
[26] L. Zhang, S. Ge, Y. Zuo, B. Zhang, L. Xi, Influence of oxygen flow rate on the morphology and magnetism of SnO2 nanostructures, J. Phys. Chem. C 114 (2010) 7541–7547.
[27] C. Wang, M. Ge, J. Jiang, Magnetic behavior of SnO2 nanosheets at room temperature, Appl. Phys. Lett. 97 (2010) 042510.
[28] T. Mahalingam, V. Dhanasekaran, R. Chandramohan, J.-K. Rhee, Microstructural properties of electrochemically synthesized ZnSe thin films, J. Mater. Sci. 47 (2012) 1950–1957.
[29] X. Li, W. Li, X. Dong, Effects of growth process on structural and optical properties of chemical bath deposition cadimium sulfide thin films, Jpn. J. Appl. Phys. 45 (2006) 9108.
[30] S. Thanikaikarasan, T. Mahalingam, K. Sundaram, A. Kathalingam, Y.D. Kim, T. Kim, Growth and characterization of electrosynthesized iron selenide thin films, Vacuum 83 (2009) 1066–1072.
[31] C. Xu, Y. Liu, G. Xu, G. Wang, Preparation and characterization of CuO nanorods by thermal decomposition of CuC 2 O 4 precursor, Mater. Res. Bull. 37 (2002) 2365–2372.
[32] Z.-s. Hong, Y. Cao, J.-F. Deng, A convenient alcohothermal approach for low temperature synthesis of CuO nanoparticles, Mater. Lett. 52 (2002) 34–38.
[33] J. Moulder, W. Sticke, P. Sobol, K. Bomben, Standard ESCA Spectra of the Elements and Line Energy Information, Handbook of X-ray Photoelectron Spectroscopy, 1992.
[34] R. Zarate, F. Hevia, S. Fuentes, V. Fuenzalida, A. Zuniga, Novel route to synthesize CuO nanoplatelets, J. Solid State Chem. 180 (2007) 1464–1469.
[35] I. Horcas, R. Fernández, J. Gomez-Rodriguez, J. Colchero, J. Gómez-Herrero, A. Baro, WSXM: a software for scanning probe microscopy and a tool for nanotechnology, Rev. Sci. Instrum. 78 (2007) 013705.
[36] E.D. Palik, Gallium Arsenide (GaAs), Handbook of Optical Constants of Solids, 1, 1985, pp. 429–443.
[37] R.A. Van Leeuwen, C.-J. Hung, D.R. Kammler, J.A. Switzer, Optical and electronic transport properties of electrodeposited thallium (III) oxide films, J. Phys. Chem. 99 (1995) 15247–15252.

[38] T. Williams, D. Hunter, A. Pradhan, I. Kityk, Photoinduced piezo-optical effect in Er doped ZnO films, Appl. Phys. Lett. 89 (2006), 43116–43116.
[39] Y.P. Sukhorukov, B.A. Gizhevskii, E.V. Mostovshchikova, A.Y. Yermakov, S.N. Tugushev, E.A. Kozlov, Nanocrystalline copper oxide for selective solar energy absorbers, Tech. Phys. Lett. 32 (2006) 132–135.
[40] S. Ovchinnikov, B. Gizhevskiĭ, Y.P. Sukhorukov, A. Ermakov, M. Uĭmin, E. Kozlov, Y.A. Kotov, A. Bagazeev, Specific features of the electronic structure and optical spectra of nanoparticles with strong electron correlations, Phys. Solid State 49 (2007) 1116–1120.
[41] D. Wu, Q. Zhang, M. Tao, LSDA+ U study of cupric oxide: electronic structure and native point defects, Phys. Rev. B 73 (2006) 235206.
[42] R. Swanepoel, Determination of the thickness and optical constants of amorphous silicon, J. Phys. E Sci. Instrum. 16 (1983) 1214.
[43] S. Devadason, M.R. Muhamad, Structural and optical properties of vapor deposited multi-layer CdSe thin films, Phys. B Condens. Matter 393 (2007) 125–132.
[44] C. Baban, G. Rusu, On the structural and optical characteristics of CdSe thin films, Appl. Surf. Sci. 211 (2003) 6–12.
[45] S. Pawar, A. Moholkar, K. Rajpure, C. Bhosale, Electrosynthesis and characterization of Fe doped CdSe thin films from ethylene glycol bath, Appl. Surf. Sci. 253 (2007) 7313–7317.
[46] A. El-Korashy, H. El-Zahed, M. Radwan, Optical studies of [N (CH 3) 4] 2 CoCl 4,[N (CH 3) 4] 2 MnCl 4 single crystals in the normal paraelectric phase, Phys. B Condens. Matter 334 (2003) 75–81.
[47] E. Marquez, A. Bernal-Oliva, J. Gonzalez-Leal, R. Prieto-Alcon, A. Ledesma, R. Jimenez-Garay, I. Martil, Optical-constant calculation of non-uniform thickness thin films of the Ge 10 As 15 Se 75 chalcogenide glassy alloy in the sub-band-gap region (0.1–1.8 eV), Mater. Chem. Phys. 60 (1999) 231–239.
[48] M. Wakkad, E.K. Shokr, S. Mohamed, Optical and calorimetric studies of Ge–Sb–Se glasses, J. Non Crystalline Solids 265 (2000) 157–166.
[49] M. DrDomenico Jr., S. Wemple, Oxygen-octahedra ferroelectrics. I. Theory of electro-optical and nonlinear optical effects, J. Appl. Phys. 40 (1969) 720–734.
[50] S. Wemple, M. DiDomenico Jr., Behavior of the electronic dielectric constant in covalent and ionic materials, Phys. Rev. B 3 (1971) 1338.
[51] S. Ilican, Y. Caglar, M. Caglar, F. Yakuphanoglu, Electrical conductivity, optical and structural properties of indium-doped ZnO nanofiber thin film deposited by spray pyrolysis method, Phys. E Low Dimensional Syst. Nanostruct. 35 (2006) 131–138.
[52] F. Karipcin, B. Dede, Y. Caglar, D. Hür, S. Ilican, M. Caglar, Y. Şahin, A new dioxime ligand and its trinuclear copper (II) complex: synthesis, characterization and optical properties, Opt. Commun. 272 (2007) 131–137.
[53] F. Yakuphanoglu, Heat treatment effect on the single oscillator parameters and optical band gap of an organic thin film, Opt. Mater. 29 (2006) 253–256.
[54] V. Dhanasekaran, T. Mahalingam, J.-K. Rhee, J. Chu, Structural and optical properties of electrosynthesized ZnSe thin films, Optik Int. J. Light Electron Opt. 124 (2013) 255–260.
[55] T. Wiktorczyk, Preparation and optical properties of holmium oxide thin films, Thin Solid Films 405 (2002) 238–242.
[56] M. Okutan, S.E. San, O. Köysal, F. Yakuphanoglu, Investigation of refractive index dispersion and electrical properties in carbon nano-balls' doped nematic liquid crystals, Phys. B Condens. Matter 362 (2005) 180–186.
[57] W. Spitzer, H. Fan, Determination of optical constants and carrier effective mass of semiconductors, Phys. Rev. 106 (1957) 882.
[58] M. Han, W. Huang, C. Chew, L. Gan, X. Zhang, W. Ji, Large nonlinear absorption in coated Ag2S/CdS nanoparticles by inverse microemulsion, J. Phys. Chem. B 102 (1998) 1884–1887.
[59] Z. Wang, V. Pischedda, S. Saxena, P. Lazor, X-ray diffraction and Raman spectroscopic study of nanocrystalline CuO under pressures, Solid state Commun. 121 (2002) 275–279.
[60] J. Xu, W. Ji, Z. Shen, S. Tang, X. Ye, D. Jia, X. Xin, Preparation and characterization of CuO nanocrystals, J. Solid State Chem. 147 (1999) 516–519.
[61] A. Tanaka, S. Onari, T. Arai, Raman scattering from CdSe microcrystals embedded in a germanate glass matrix, Phys. Rev. B 45 (1992) 6587.
[62] J. Coey, M. Venkatesan, C. Fitzgerald, Donor impurity band exchange in dilute ferromagnetic oxides, Nat. Mater. 4 (2005) 173–179.
[63] A. Punnoose, H. Magnone, M. Seehra, J. Bonevich, Bulk to nanoscale magnetism and exchange bias in CuO nanoparticles, Phys. Rev. B 64 (2001) 174420.
[64] S.D. Yoon, Y. Chen, A. Yang, T.L. Goodrich, X. Zuo, D.A. Arena, K. Ziemer, C. Vittoria, V.G. Harris, Oxygen-defect-induced magnetism to 880 K in semiconducting anatase TiO2− δ films, J. Phys. Condens. Matter 18 (2006) L355.
[65] V. Bisht, K. Rajeev, S. Banerjee, Anomalous magnetic behavior of CuO nanoparticles, Solid State Commun. 150 (2010) 884–887.
[66] M. Ghosh, K. Biswas, A. Sundaresan, C. Rao, MnO and NiO nanoparticles: synthesis and magnetic properties, J. Mater. Chem. 16 (2006) 106–111.
[67] S. Tiwari, K. Rajeev, Signatures of spin-glass freezing in NiO nanoparticles, Phys. Rev. B 72 (2005) 104433.
[68] A. Sundaresan, R. Bhargavi, N. Rangarajan, U. Siddesh, C. Rao, Ferromagnetism as a universal feature of nanoparticles of the otherwise nonmagnetic oxides, Phys. Rev. B Condens. Matter Mater. Phys. 74 (2006), 161306_161301-161306_161304.
[69] N. Sanchez, S. Gallego, M. Munoz, Magnetic states at the oxygen surfaces of ZnO and Co-doped ZnO, Phys. Rev. Lett. 101 (2008) 067206.